

# Simultaneous Determination of the Cosmic Ray Ionization Rate and Fractional Ionization in DR21(OH)

Talayeh Hezareh<sup>1</sup>,

hezareh@astro.uwo.ca

Martin Houde<sup>1</sup>, Carolyn M<sup>c</sup>Coey<sup>1,2</sup>, Charlotte Vastel<sup>3</sup>,

and

Ruisheng Peng<sup>4</sup>

## ABSTRACT

We present a new method for the simultaneous calculation of the cosmic ray ionization rate,  $\zeta_{\text{H}_2}$ , and the ionization fraction,  $\chi_e$ , in dense molecular clouds. A simple network of chemical reactions dominant in the creation and destruction of  $\text{HCNH}^+$  and  $\text{HCO}^+$  is used in conjunction with observed pairs of rotational transitions of several molecular species in order to determine the electron abundance and the  $\text{H}_3^+$  abundance. The cosmic ray ionization rate is then calculated by taking advantage of the fact that, in dark clouds, it governs the rate of creation of  $\text{H}_3^+$ . We apply this technique to the case of the star-forming region DR21(OH), where we successfully detected the ( $J = 3 \rightarrow 2$ ) and ( $J = 4 \rightarrow 3$ ) rotational transitions of  $\text{HCNH}^+$ . We also determine the C and O isotopic ratios in this source to be  $^{12}\text{C}/^{13}\text{C} = 63 \pm 4$  and  $^{16}\text{O}/^{18}\text{O} = 318 \pm 64$ , which are in good agreement with previous measurements in other clouds. The significance of our method lies in the ability to determine  $N(\text{H}_3^+)$  and  $\chi_e$  directly from observations, and estimate  $\zeta_{\text{H}_2}$  accordingly. Our results,  $\zeta_{\text{H}_2} = 3.1 \times 10^{-18} \text{ s}^{-1}$  and  $\chi_e = 3.2 \times 10^{-8}$ , are consistent with recent determinations in other objects.

*Subject headings:* ISM: cloud — ISM: molecules — ISM: cosmic rays

---

<sup>1</sup>The Department of Physics and Astronomy, The University of Western Ontario, London, Ontario, Canada N6A 3K7

<sup>2</sup>Department of Physics and Astronomy, University of Waterloo, 200 University Avenue W., Ontario, Canada N2L 3G1

<sup>3</sup>Centre d'Etude Spatiale des Rayonnements, 9 avenue du colonel Roche BP 44346, 31028 Toulouse Cedex 4, FRANCE

<sup>4</sup>Caltech Submillimeter Observatory, 111 Nowelo Street, Hilo, HI 96720

## 1. Introduction

The ionization fraction (or the electron abundance),  $\chi_e \equiv n(e)/n(\text{H}_2)$ , where  $n(e)$  is the electron number density and  $n(\text{H}_2)$  the hydrogen molecule number density, plays a key role in the chemistry and dynamics of dense molecular clouds. Due to the low temperatures within dense clouds, the chemistry is dominated by reactions between ions and neutral species. Furthermore, if a magnetic field permeates the cloud, the ions interact directly with the field through the Lorentz force, while the rate of collisions between the ions and the neutral species determines the degree with which the neutral gas couples to the magnetic field. The ionization fraction therefore determines the strength of this coupling, and hence the ambipolar diffusion timescale in a molecular cloud, which is a measure of the stability of the cloud against gravitational collapse (Shu 1992). Moreover, determination of the fractional ionization can be essential in precisely estimating the magnetic strength in molecular clouds (Li & Houde 2008).

In order to determine the ionization fraction in a cloud, it is important to identify the main ionization processes in the region under study. Star formation occurs in dense cores, which are regions of high extinction where self-shielding prevents the UV photo-ionization of  $\text{H}_2$ . It is also expected that X-ray ionization is only significant in the vicinity of strong X-ray sources such as active galactic nuclei (McCall et al. 1999) and OB stars. Therefore, cosmic ray ionization is believed to dominate photo-ionization in dense cores (McKee 1989).

Cosmic rays also heat the interstellar gas and drive interstellar chemistry in dense molecular clouds. Direct determination of the cosmic ray ionization rate,  $\zeta_{\text{H}_2}$ , is achievable by studying the abundance of  $\text{H}_3^+$  due to the relative simplicity of its chemistry (McCall et al. 1999). This important molecule is created via cosmic ray ionization of the  $\text{H}_2$  molecule, and is highly reactive with electrons and neutral species present in such clouds. For example, it reacts with HCN, CO and  $\text{N}_2$  to form  $\text{HCNH}^+$ ,  $\text{HCO}^+$  and  $\text{N}_2\text{H}^+$ , respectively. The resulting ions react with different neutral molecules, producing other ionic or neutral species. For this study, we assume that  $\text{H}_3^+$  is mainly produced by cosmic rays.

Various techniques have been developed in the past to estimate the ionization fraction and cosmic ray ionization rate. For the prior, there have been studies that based its determination on measurements of the degree of deuterium fractionation through  $\text{DCO}^+$  and  $\text{HCO}^+$  abundance ratios (e.g., Caselli et al. 1998). The application of this technique in cold clouds is limited, since the freeze-out of molecules onto the grain surfaces affects the degree of deuterium fractionation independently of the ionization fraction (Caselli et al. 1998). Observations of  $\text{H}_3^+$  absorption lines (McCall et al. 1999) together with appropriate chemical models have been used for the determination of  $\zeta_{\text{H}_2}$  in diffuse clouds and envelopes of molecular clouds (van der Tak & van Dishoeck 2000; Indriolo et al. 2007). However, this method

is not applicable to cold starless cores since  $\text{H}_3^+$  has no electric dipole moment; it cannot be used to trace such regions.

In dense cores, typical values for  $\zeta_{\text{H}_2}$  are estimated to be  $(1 - 5) \times 10^{-17} \text{ s}^{-1}$  (Dalgarno 2006), while the fractional ionization is found to lie within a small range,  $10^{-7.3} \lesssim \chi_e \lesssim 10^{-6.9}$  (Bergin et al. 1999). However, some recent studies have found lower values for these parameters in dark clouds. For example, Maret & Bergin (2007) obtained a fractional ionization of  $5 \times 10^{-9}$  with respect to H nuclei corresponding to a cosmic ray ionization of  $(1 - 6) \times 10^{-18} \text{ s}^{-1}$  in the Barnard 68 prestellar core, while Flower et al. (2007) reported  $n_e/n_{\text{H}} = 1 \times 10^{-8}$  and  $\zeta_{\text{H}_2} = 2 \times 10^{-18} \text{ s}^{-1}$  in TMC-1. Since the two parameters are interdependent, one is usually determined by restricting the other through fitting theoretical models to observations (see for example, Wootten et al. 1979; Plume et al. 1998).

In this work we show that it is possible to estimate the cosmic ray ionization rate and fractional ionization simultaneously, using observational spectroscopic data together with a simple network of chemical reactions that involve  $\text{H}_3^+$  and the electron abundance. These reactions are responsible for the formation and destruction of well-studied molecular species that co-exist in dense molecular clouds. Accordingly, we chose to study  $\text{HCNH}^+$  and  $\text{HCO}^+$  and applied this technique to the star-forming region DR21(OH).

We explain the observational procedure in §2 and present our technique in §3. Our numerical calculations and results are described in §4, followed by a discussion and summary in §5.

## 2. Observations

### 2.1. Source description

DR21(OH) ( $\alpha = 20^{\text{h}}39^{\text{m}}01^{\text{s}}$  and  $\delta = 42^{\circ}22'37.7''$ , J2000) is located about  $3'$  to the north of DR21, a well-known massive star formation site in the Cygnus X region that lies at a distance of approximately 3 kpc (Genzel & Downes 1977). Also known as W75S, it is made up of several compact sources, namely DR21(OH)Main, DR21(OH)N, DR21(OH)S and DR21(OH)W, which are all active star-forming regions (Curran et al. 2005). This work is focused on the brightest component, DR21(OH)Main. Continuum studies have detected two dense cores, MM1 and MM2, with a total mass of about  $125 M_{\odot}$  in the center of DR21(OH)Main (Woody et al. 1989). This source has been extensively studied in the infrared and also mapped in CO (Dickel et al. 1978; Magnum et al. 1991), and no young stars with strong radiation fields have been observed around it (Davis et al. 2007). Also, no centimeter-wavelength continuum sources have been detected within the source, suggesting

a lack of HII regions (Johnston et al. 1984), implying that it is in an early stage of evolution and thus suitable for our analysis.

## 2.2. Spectroscopic data

We obtained all observations at the Caltech Submillimeter Observatory (CSO), located on Mauna Kea, Hawaii. In Table 1, we list the detections of different rotational transitions from the molecular species that form the main creation and destruction routes for  $\text{HCNH}^+$  and  $\text{HCO}^+$  (see §3). Among these molecules,  $\text{HCO}^+$ ,  $\text{CO}$ ,  $\text{HCN}$  and  $\text{HNC}$  were optically thick, and therefore not suitable for our analysis. Instead, we observed the optically thin isotopologues  $\text{H}^{13}\text{CO}^+$ ,  $\text{H}^{13}\text{CN}$  and  $\text{HN}^{13}\text{C}$ , as well as  $^{12}\text{C}^{18}\text{O}$ ,  $^{13}\text{C}^{18}\text{O}$ , and  $^{13}\text{C}^{16}\text{O}$  in order to determine the  $^{12}\text{C}/^{13}\text{C}$  and  $^{16}\text{O}/^{18}\text{O}$  isotopic ratios needed for the calculation of the abundance of the main species from their observed isotopologues.

In October 2006, we detected  $\text{HCNH}^+$  in the  $J = 3 \rightarrow 2$  and  $J = 4 \rightarrow 3$  transitions in DR21(OH)Main using the 200-300 GHz receiver. For these observations, standard telescope efficiencies of 66 % at 222 GHz (beam width  $\sim 33''$ ) and 60 % at 296 GHz (beam width  $\sim 25''$ ) were used. Data were taken in a position switching mode and the pointing was checked regularly using scans on Uranus.  $\text{H}^{13}\text{CO}^+$  and  $\text{H}^{13}\text{CN}$  were observed during the months of October, November and December 1999, using the 200-300 GHz and 300-400 GHz receivers. These spectra were calibrated using scans made on planets available during that period (Mars, Jupiter and Saturn). The telescope efficiencies were  $\sim 70$  % for the 200-300 GHz receiver (beam width of  $\sim 32''$ ) and  $\sim 60$  % for the 300-400 GHz receiver (beam width of  $\sim 20''$ ) (Houde et al. 2000).

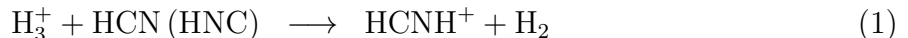
We obtained the final set of observational data required for this analysis in October and November 2007. During that period, the  $^{12}\text{C}^{18}\text{O}$ ,  $^{13}\text{C}^{18}\text{O}$ , and  $^{13}\text{C}^{16}\text{O}$  molecular species were detected in two rotational transitions ( $J = 2 \rightarrow 1$  and  $J = 3 \rightarrow 2$ ) towards the center position of DR21(OH). We also attempted to detect  $\text{H}_3\text{O}^+$  in  $J = 3_0 \rightarrow 2_0$  and  $J = 3_2 \rightarrow 2_2$  transitions at 396 GHz and 364 GHz, respectively. Although we were successful in detecting the 364 GHz transition, we did not record an acceptable detection for the 396 GHz transition. Standard telescope efficiencies were also used for these sets of data (i.e.,  $\sim 66$  % at 200-300 GHz with a beam width of  $\sim 33''$ , and  $\sim 58$  % at 300-400 GHz with a beam width of  $\sim 22''$ ). Figure 1 shows the spectra for  $\text{HCNH}^+$  and  $\text{H}_3\text{O}^+$ . The spectra for the  $J = 3 \rightarrow 2$  and  $J = 4 \rightarrow 3$  transitions of  $\text{H}^{13}\text{CO}^+$ ,  $\text{H}^{13}\text{CN}$  and  $\text{HN}^{13}\text{C}$  are shown in Figure 2, while the detections of the CO isotopologues are presented in Figure 3. All the data reduction was

carried out using the GILDAS<sup>1</sup> and CASSIS<sup>2</sup> software packages.

DR21(OH) is well known to have a multiply peaked structure, suggesting that the cloud is in an early stage of massive star formation (Richardson et al. 1994). Therefore, it is important to determine whether or not the emission from the molecules under study arises from the same volume of gas along the line of sight. In order to confirm the coexistence of the molecular species along each line of sight, it is useful to obtain velocity maps and analyze them together with line profiles. However, velocity mapping, especially for the faint lines of HCNH<sup>+</sup> and H<sub>3</sub>O<sup>+</sup>, required a longer integration time than was available to us. Nevertheless, consideration of the spectra in Figures 1, 2 and 3 shows an alignment of the peak velocities of the detected lines near -3 km s<sup>-1</sup>. Therefore, to a good approximation, the observed molecular species are coexistent in the region along our line of sight. Notable exceptions are the  $J = 4 \rightarrow 3$  transition of HN<sup>13</sup>C and  $J = 3 \rightarrow 2$  transition of <sup>12</sup>C<sup>18</sup>O in Figure 2 and 3, respectively. The corresponding observations are, therefore, not used in our analysis.

### 3. Method

In this section, we describe the main creation and destruction paths of HCNH<sup>+</sup> and HCO<sup>+</sup> in dense clouds and the method used to calculate  $n(e)$ ,  $n(\text{H}_3^+)$  and  $\zeta_{\text{H}_2}$ . In dense clouds, the chemistry is dominated by ion-neutral reactions and the main formation reactions for HCNH<sup>+</sup> are as follows (Schilke et al. 1991)



Likewise, in dark clouds, HCO<sup>+</sup> is mainly formed by the reaction of H<sub>3</sub><sup>+</sup> with CO (Herbst & Klemperer 1973; Watson 1974)

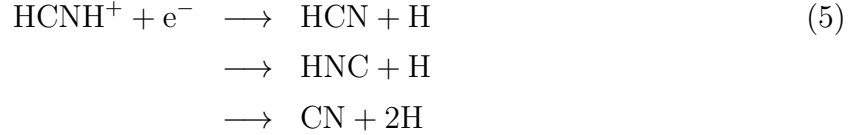



---

<sup>1</sup>URL: <http://iram.fr/IRAMFR/GILDAS/>

<sup>2</sup>URL: <http://cassis.cesr.fr/>

Both  $\text{HCNH}^+$  and  $\text{HCO}^+$  are mainly removed through dissociative recombination with electrons (Schilke et al. 1991; Plume et al. 1998)



The rate coefficients of the above reactions are taken from the UMIST database (Woodall et al. 2007) and are listed in Table 2. The kinetic temperature in dark molecular clouds is usually between 10 to 40 K; we follow Wilson & Mauersberger (1990) in adopting a kinetic temperature of 20 K for DR21(OH) to evaluate these rate coefficients.

There are several other reactions that can contribute to the creation and destruction of  $\text{HCNH}^+$  and  $\text{HCO}^+$  in dense clouds, but they can safely be neglected due to their low rate coefficients and/or the relatively low abundance of the molecules involved (e.g., reactions involving  $\text{C}_2\text{H}_2^+$ ,  $\text{H}_2\text{O}^+$ ,  $\text{H}_2\text{CO}^+$ ,  $\text{HNO}^+$ ,  $\text{C}_2^+$ , and  $\text{H}_2\text{S}^+$ ).

We can use the aforementioned reactions to equate the rates of formation and destruction of  $\text{HCNH}^+$  (equations (1)-(3), and (5)) and  $\text{HCO}^+$  (equations (4) and (6)) to obtain the following expressions for the electron and  $\text{H}_3^+$  abundances

$$n(e) = \frac{[n(\text{HCN}) + n(\text{HNC})][n(\text{H}_3^+)k_1 + n(\text{HCO}^+)k_2 + n(\text{H}_3\text{O}^+)k_3]}{n(\text{HCNH}^+)k_5}, \quad (7)$$

$$n(\text{H}_3^+) = \frac{n(\text{HCO}^+)n(e)k_6}{n(\text{CO})k_4}. \quad (8)$$

Since we have obtained all the observations necessary to determine the abundance of the HCN, HNC,  $\text{HCO}^+$ ,  $\text{H}_3\text{O}^+$ ,  $\text{HCNH}^+$ , and CO molecular species, we are left with a set of two equations and two unknowns (i.e.,  $n(\text{H}_3^+)$  and  $n(e)$ ). It will therefore be straightforward to simultaneously determine  $n(\text{H}_3^+)$  and  $n(e)$  using equations (7) and (8) and our spectroscopic data.

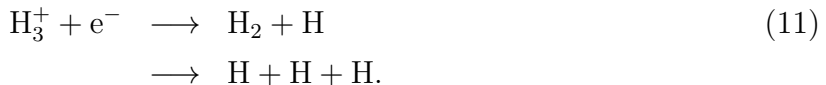
The cosmic ray ionization rate can be obtained directly from the abundance of  $\text{H}_3^+$ , which forms as follows (Solomon & Werner 1971; Bowers et al. 1969)





The reaction between  $\text{H}_2^+$  and  $\text{H}_2$  proceeds very rapidly (Solomon & Werner 1971) and is limited by the abundance of  $\text{H}_2^+$ . The rate of formation of  $\text{H}_3^+$  is therefore governed by the ionization of  $\text{H}_2$  by cosmic rays.

The main destruction path for  $\text{H}_3^+$  in dense cores is through reactions with CO (McCall et al. 1999), due to the high reaction rate and the fact that the latter has the highest fractional abundance with respect to  $\text{H}_2$  in molecular clouds. Furthermore,  $\text{H}_3^+$  is also destroyed by dissociative recombination with electrons through



Although the overall rate for this reaction is an order of magnitude lower than that involving CO (see equation (4)), we still include it in what follows for completeness. Again, assuming statistical equilibrium between the formation and destruction rate of  $\text{H}_3^+$ , we obtain

$$\zeta_{\text{H}_2} = \frac{n(\text{H}_3^+)n(\text{CO})k_4 + n(\text{H}_3^+)n(\text{e})k_{11}}{n(\text{H}_2)}. \quad (12)$$

The main advantage of our method is that it enables us to calculate  $\chi_e$  and  $\zeta_{\text{H}_2}$  simultaneously through equations (7), (8) and (12), without the need to consider more extensive chemical networks for each molecular species involved. As mentioned before, this is because the required abundances are determined directly from observations. This feature differentiates ours from previous techniques.

## 4. Results

The expressions for  $\chi_e$  and  $\zeta_{\text{H}_2}$  in the previous section are couched in terms of abundance but could equivalently be written in terms of column density, which is a more natural quantity to use when analyzing observation. We calculated the excitation temperature of every observed molecular species (or at least for one of its isotopologues) that appears in equations (7) and (8) in order to calculate its column density. The C and O isotopic ratios in the cloud were determined with observations of the  $^{12}\text{C}^{18}\text{O}$ ,  $^{13}\text{C}^{18}\text{O}$  and  $^{13}\text{C}^{16}\text{O}$  molecular species, and were used to evaluate the column density of the common molecular species (more below).

#### 4.1. Excitation temperatures and column densities

We determined the excitation temperatures and column densities of the observed molecules using a LTE approach. For this purpose, we detected two transitions for each molecular species and obtained the ratio of their integrated intensities (Blake et al. 1987; Emerson 1996). The brightness temperature of a source can be written as (Kutner & Ulich 1981)

$$T_b(\nu) = T_0 \left[ \frac{1}{e^{(T_0/T_{ex})} - 1} - \frac{1}{e^{(T_0/T_{\text{CMB}})} - 1} \right] (1 - e^{-\tau(\nu)}), \quad (13)$$

where  $T_{ex}$  is the excitation temperature,  $T_{\text{CMB}}$  the cosmic microwave background brightness temperature (2.7 K),  $\tau(\nu)$  the optical depth, and  $T_0 = h\nu/k$ , with  $\nu$  the frequency. The term involving the background brightness temperature is insignificant compared to the other term and is therefore neglected. The mean optical depth can be written as a function of column density as

$$\begin{aligned} \tau \Delta v &\equiv \int \tau(v) dv \\ &= \frac{A_{ul} c^3 N_u}{8\pi \nu^3} (e^{(T_0/T_{ex})} - 1), \end{aligned} \quad (14)$$

where  $\Delta v$  is the extent of the spectral line,  $A_{ul}$  is the Einstein coefficient for spontaneous emission (listed in Table 1) and  $N_u$  is the column density of the upper level of a transition, which, in turn, can be written as a function of the integrated brightness temperature and mean optical depth of the line as

$$N_u = \frac{8\pi k \nu^2}{h c^3 A_{ul}} \left( \frac{\tau}{1 - e^{-\tau}} \right) \int T_b dv, \quad (15)$$

where the term  $\int T_b dv$  is the integrated intensity of the spectral line profile and the term  $\tau/(1 - e^{-\tau})$  (hereafter abbreviated by  $\beta$ ) is the optical depth correction factor (Langer & Penzias 1993). For optically thin lines, where  $\tau \ll 1$ ,  $\beta$  approaches unity. Within the LTE approximation, the population of the levels is assumed to be thermalized and the total column density of the molecular species along the observer's line of sight,  $N_{tot}$ , can be expressed as

$$N_{tot} = \frac{8\pi k \nu^2 U(T_{ex})}{h c^3 A_{ul} g_u} e^{(E_u/kT_{ex})} \beta \int T_b dv, \quad (16)$$

where  $U(T_{ex})$  is the partition function at the excitation temperature  $T_{ex}$ , while  $g_u$  and  $E_u$  are the upper state degeneracy and energy, respectively.



In order to obtain the excitation temperature of a molecular species that exhibits optically thin line profiles, we obtained the ratio of the integrated intensities of its two observed transitions using equation (16). For such molecules, we adopted  $\beta = 1$  for the corresponding spectral lines and solved for  $T_{ex}$ , assuming it to be the same for both transitions. The optical depths of the lines were subsequently calculated using equation (14). For example, in the case of  $\text{H}^{13}\text{CN}$  we obtained a  $T_{ex}$  of 13 K and opacities of 0.09 and 0.06 for the  $J = 3 \rightarrow 2$  and  $J = 4 \rightarrow 3$  transitions, respectively. The optical depths for all transitions thus calculated are listed in Table 1. This method could not be used for  $^{12}\text{C}^{18}\text{O}$  and  $^{13}\text{C}^{16}\text{O}$ , as their transitions are not optically thin.

Inspection of the  $^{12}\text{C}^{18}\text{O}$  spectra in Figure 3 reveals that the line profiles are slightly saturated. Furthermore, the peak velocity of the  $J = 3 \rightarrow 2$  transition is clearly blue-shifted from the  $J = 2 \rightarrow 1$  transition and the vast majority of the other observed lines rendering it unsuitable for this analysis, since it possibly arises from a different region. Therefore, care had to be taken toward the determination of the excitation temperature and optical depth of this molecule. Since the line profile for the  $J = 2 \rightarrow 1$  transition is relatively symmetric and of appropriate shape, we fitted it with a Gaussian profile. We then used the equation for a Gaussian line from Vastel (2006) and Newton’s method to numerically solve the equation

$$N_u - \frac{8\pi k\nu^2}{hc^3 A_{ul}} \left( \frac{\tau(N_u)}{1 - e^{-\tau(N_u)}} \right) T_b \delta v = 0 \quad (17)$$

for  $N_u$  and subsequently for  $\tau(N_u)$  for a very narrow velocity interval  $\delta v$  centered on  $v$ . The dependency of the mean optical depth on  $N_u$  follows from equation (14). This way, we obtained the optical depth in different parts of the line profile to model the spectrum using a range of excitation temperatures ( $10 < T_{ex} < 25$ ). Every optical depth value was converted to a brightness temperature using equation (13) and consequently, assuming a beam filling factor of 1, to an antenna temperature through  $T_A^* = \eta T_b$ , where  $\eta$  is the telescope efficiency at the appropriate frequency. The excitation temperature of  $^{12}\text{C}^{18}\text{O}$  was taken to be the temperature of the best fit to the  $J = 2 \rightarrow 1$  spectrum. The line profiles of  $\text{H}_3\text{O}^+$  ( $J = 3_2 \rightarrow 2_2$ ) and  $\text{HN}^{13}\text{C}$  ( $J = 3 \rightarrow 2$ ) were modelled in a similar fashion to obtain their excitation temperatures, since these were the only credible transitions detected for these molecules.

The  $^{13}\text{C}^{16}\text{O}$  lines are optically thick, as is made clear from their self-absorbed profiles (see Figure 3). In order to obtain the excitation temperature for  $^{13}\text{C}^{16}\text{O}$ , we took the ratio of the integrated intensities in the wings of the line profiles, where the line optical depth is small ( $\beta \sim 1$ ) and applied the method described above.

Finally, the column densities of all molecules, except  $^{13}\text{C}^{16}\text{O}$  and  $^{12}\text{C}^{16}\text{O}$ , were calculated

using equation (16) and the values of  $\tau$  and  $T_{ex}$  as explained above. These results are summarized in Table 3 (the cases of  $^{13}\text{C}^{16}\text{O}$  and  $^{12}\text{C}^{16}\text{O}$  are considered in the next section). The excitation temperatures obtained for the different species fall in a narrow range of 12 to 22 K, which is consistent with the assumption of LTE and the kinetic temperature of 20 K discussed in §3.

#### 4.2. C and O isotopic ratios

The  $^{12}\text{C}/^{13}\text{C}$  isotopic ratio was directly determined from the ratio of the column density of  $^{12}\text{C}^{18}\text{O}$  to that of  $^{13}\text{C}^{18}\text{O}$ . The observation of these relatively low-abundance species has the advantage of probing denser regions over the observation of more abundant isotopologues such as  $^{12}\text{C}^{16}\text{O}$  and  $^{13}\text{C}^{16}\text{O}$ .

For the carbon isotopic ratio, we obtain

$$\frac{^{12}\text{C}}{^{13}\text{C}} \equiv \frac{N_{tot}(^{12}\text{C}^{18}\text{O})}{N_{tot}(^{13}\text{C}^{18}\text{O})} = 63 \pm 4, \quad (18)$$

which is consistent with the results of Langer & Penzias (1993) in other clouds.

In order to determine the  $^{16}\text{O}/^{18}\text{O}$  isotopic ratio, it was necessary to compare the abundance of  $^{13}\text{C}^{16}\text{O}$  with that of  $^{13}\text{C}^{18}\text{O}$ . Since the  $^{13}\text{C}^{16}\text{O}$  profiles show self-absorption, we took the intensity ratio,  $R$ , of the  $J = 2 \rightarrow 1$  transitions of  $^{13}\text{C}^{16}\text{O}$  and  $^{12}\text{C}^{18}\text{O}$  in a common velocity interval in the wings, where the line opacities are relatively small (we included the optical depth correction,  $\beta$ , for  $^{13}\text{C}^{16}\text{O}$  in this ratio). There is an uncertainty in the obtained value for the column density of  $^{13}\text{C}^{16}\text{O}$ , since  $R$  may vary over the line profile. Nevertheless, we examined this ratio in two different parts of each wing in order to check its consistency. The  $^{16}\text{O}/^{18}\text{O}$  isotopic ratio is determined to be

$$\frac{^{16}\text{O}}{^{18}\text{O}} \equiv \beta R \left( \frac{^{12}\text{C}}{^{13}\text{C}} \right) = 318 \pm 64, \quad (19)$$

which is in agreement with previous studies in other clouds (Penzias 1981; Polehampton et al. 2005).

The column densities of the species listed in Table 3 were then calculated from their isotopologues using the obtained C and O isotopic ratios. We determined the column density of  $^{13}\text{C}^{16}\text{O}$  and  $^{12}\text{C}^{16}\text{O}$  and estimated the column density of molecular hydrogen in DR21(OH) to be (Stahler & Palla 2004)

$$N(\text{H}_2) \simeq 3.8 \times 10^5 N(^{13}\text{CO}) \simeq 1.1 \times 10^{23} \text{ cm}^{-2}. \quad (20)$$

### 4.3. Fractional ionization and cosmic ray ionization rate

We determined the  $\text{H}_3^+$  and electron abundances for DR21(OH) using the column density equivalent of equations (7) and (8), and equation (20). For the fractional ionization and  $\text{H}_3^+$  column density we report  $\chi_e = 3.2 \times 10^{-8}$  and  $N(\text{H}_3^+) = 5.5 \times 10^{13} \text{ cm}^{-2}$ , respectively. McCall et al. (1999) detected absorption lines of  $\text{H}_3^+$  in several dense molecular clouds, and estimated  $N(\text{H}_3^+)$  to be  $(1 - 5) \times 10^{14} \text{ cm}^{-2}$ . We find our calculated value for  $N(\text{H}_3^+)$  lower than theirs. Our result for  $\chi_e$  agrees well with previous findings in other sources (Bergin et al. 1999; Flower et al. 2007). Moreover, we estimate the cosmic ray ionization rate for DR21(OH)Main to be  $\zeta_{\text{H}_2} = 3.1 \times 10^{-18} \text{ s}^{-1}$  through equation (12), which agrees with recent results for other clouds (e.g., Flower et al. 2007).

It should be noted that the rate coefficients for the chemical reactions are either calculated or measured in laboratories, and have uncertainties ranging from 25% up to a factor of 2 (Woodall et al. 2007). The OSU database has historically been used for chemical modelling of dark clouds; however, the latest release of the UMIST database contains dipole reactions with fits specific for low temperatures and is well-suited to this type of modelling. The difference in the rate coefficients between the two databases are within a factor of two and, in order to investigate the effect of this, we repeated our calculations using the rate coefficients from the OSU database. We find an increase in the ionization fraction and the cosmic rate ionization rate by a factor of two, which is commensurate with the uncertainties in the rate coefficients mentioned above.

The cloud size along the line of sight is needed for the calculation of the molecular number densities, and can be approximately estimated through the inspection of extended emission maps of molecules in the cloud. But the uncertainty in the distance of the source adds to the inaccuracy in the determination of the cloud size. We estimated the cloud size from the HCN ( $J = 4 \rightarrow 3$ ) map by Richardson et al. (1986) to be 1.7 pc. Finally, the column density of molecular hydrogen in dense clouds is usually calculated using standard ratios of CO/ $\text{H}_2$  or through extinction measurements. All the uncertainties in the aforementioned parameters cause  $\zeta_{\text{H}_2}$  to be uncertain by a factor of a few.

## 5. Discussion and Summary

We have presented a simple yet novel method to simultaneously estimate the ionization fraction and cosmic ray ionization rate of  $\text{H}_2$  in dense molecular clouds. These parameters were determined in DR21(OH) using ancillary observational data pertaining to the formation and destruction reactions of  $\text{HCNH}^+$  and  $\text{HCO}^+$ , which involve the  $\text{H}_3^+$  and electron abundance. We have made a number of assumptions regarding this method, which will be discussed here.

a) The primary assumption in this method is that cosmic rays are the dominant means of ionization in DR21(OH). As mentioned earlier, there has been no detection of HII regions in DR21(OH), which implies there are no actively photo-ionizing stars in the cloud. Gibb et al. (2005) mapped the DR21/DR21(OH) region at 3 mm, 850  $\mu\text{m}$  and 450  $\mu\text{m}$  and identified several submillimeter sources within the region, which only suggest the existence of deeply embedded young protostars in the source. We note that the value we obtain for the ionization fraction is consistent with our assumption.

b) We selected the most significant formation and destruction routes for  $\text{HCNH}^+$  and  $\text{HCO}^+$  by identifying the reactions that had the largest rate coefficients and involved significantly abundant molecules. There are other ionic and neutral species such as  $\text{CO}^+$ ,  $\text{C}^+$ ,  $\text{HCN}^+$ , and  $\text{H}_2\text{O}$  that take part in the  $\text{HCNH}^+$  and  $\text{HCO}^+$  chemistry. These species are abundant in photon dominated regions (Savage & Ziurys 2004), but can safely be neglected here given the lack of photo-ionizing sources in DR21(OH), as noted above.

c) For our calculations, we have assumed chemical equilibrium within the region under study. Lintott & Rawlings (2006) argue that in a rapidly evolving cloud, the dynamical timescale may be shorter than the chemical timescale, and hence chemical equilibrium will not be established until the cloud has reached a quiescent stage, i.e., passed its initial collapse phase. They mention this timescale to be on the order of  $10^6$  years. If chemical equilibrium is not met in DR21(OH), then  $\zeta_{\text{H}_2}$  will be overestimated by a factor of 2 – 3 (Lintott & Rawlings 2006). This uncertainty is comparable with the uncertainties in the rate coefficients, observational calibrations, and measurements of cloud size and molecular hydrogen abundance.

d) DR21(OH) is known to harbor water and methanol masers (associated with the MM1 and MM2 continuum sources), being an indication of the presence of outflows within the source. Magnum et al. (1991, 1992) observed this source using the VLA and found an excitation temperature above 80 K within a region of  $\sim 10''$  centered on MM1 (VLSR  $\sim -4.1 \text{ km s}^{-1}$ ). Gas associated with such regions would understandably have different physical characteristics compared to the more extended, relatively quiescent regions probed with our

observations. It is the latter that dominates the region we observed with our larger telescope beam ( $\sim 20''$  to  $\sim 30''$ ). Nevertheless, previous studies have established that this star-forming region possesses a complex structure owing to the presence of deeply embedded sources, and the detection of molecular masers further supports this conclusion. One could thus question our assignment of a single kinetic temperature of 20 K for DR21(OH). But since we obtained a narrow range of temperatures (12 - 22 K) for all the molecular species we observed, we believe that our aforementioned chosen value is justified for the spatial resolution attained with our observations. Incidentally, this narrow range of temperatures for all species is also consistent with the use of the LTE approximation for this study.

Provided the above assumptions are met, our method will be very useful for the calculation of  $\chi_e$  and  $\zeta_{\text{H}_2}$  in dense molecular clouds without the need for detailed chemical models. However, the application of this technique can be limited due to the likely difficulty in detecting  $\text{HCNH}^+$ . For example, we attempted to observe  $\text{HCNH}^+$  in other molecular clouds such as W3(OH), AFGL2591 and AFGL490 but could not record any credible detection. For these situations, other molecules such as  $\text{HCS}^+$ , whose formation and destruction follow a similar chemistry and could be coexistent with  $\text{HCO}^+$  may be taken into consideration.

Moreover, it is not straightforward to precisely determine the density for which our values of the ionization fraction and cosmic ray ionization rate apply when one considers that our array of observations involves molecules with a vast range of critical densities (e.g., from  $\sim 10^3 \text{ cm}^{-3}$  for CO to  $\sim 10^8 \text{ cm}^{-3}$  for HCN). We had to assume that all observed species are coexistent within DR21(OH) in order to carry our program; however, this is probably not strictly accurate. This is especially the case for CO and its isotopologues, because of their lower critical densities, and this brings a further uncertainty in our determination of  $\chi_e$  and  $\zeta_{\text{H}_2}$ . Unfortunately, it is difficult to evaluate the magnitude of this bias with our existing data. On the other hand, the good alignment of spectral peak intensities and the relative agreement on excitation temperatures is consistent with our coexistence approximation.

Although our method does not take account of gas-grain interactions or deuterated species, which may be important for clouds at very low temperatures (e.g. Flower et al. 2007), its simplicity and reliance on observations render it a powerful tool for the simultaneous calculation of  $\chi_e$  and  $\zeta_{\text{H}_2}$ . Moreover, this method enables us to indirectly estimate the column density of  $\text{H}_3^+$  in dense molecular clouds. This is important, since the low abundance of  $\text{H}_3^+$  makes its absorption lines difficult to observe, and it is not at all detectable in the submillimeter regime. Furthermore, the obtained values for  $\chi_e$  and  $\zeta_{\text{H}_2}$  are applicable in the calculations of ambipolar diffusion timescale and the magnitude of the mean magnetic field in the cloud, which will be addressed in a future paper.

The authors thank the anonymous referee for a careful reading and insightful comments, and also D. Johnstone and J. Di Francesco for helpful discussions and suggestions. M. H.'s research is funded through the NSERC Discovery Grant, Canada Research Chair, Canada Foundation for Innovation, Ontario Innovation Trust, and Western's Academic Development Fund programs. The Caltech Submillimeter Observatory is funded through the NSF grant AST 05-40882 to the California Institute of Technology.

## REFERENCES

- Bergin, E. A., Plume, R., Williams, J. P., & Myers, P. C. 1999, *ApJ*, 512, 724
- Blake, G. A., Sutton, E. C., Masson C. R., & Phillips T. G. 1987, *ApJ*, 315, 621
- Bowers, M. T., Elleman, D. D., & King, J. 1969, *J. Chem. Phys.*, 50, 4787
- Caselli, P., Walmsley, C. M., Terzieva, R., & Herbst, E. 1998, *ApJ*, 499, 234
- Curran, R. L., Collett, J. L., Atkinson, J. W., Chrysostomou, A., & Aitken, D. K. 2005, *Protostars and Planets V*, 8160
- Dalgarno, A. 2006, *PNAS*, 103, 33, 12269
- Davis, C. J., Kumar, M. S. N., Sandell, G., Froebrich, D., Smith, M. D., & Currie, M. J. 2007, *MNRAS*, 374, 29
- Dickel, H., Dickel, J., & Wilson, W. 1978, *ApJ*, 223, 840
- Emerson, D. 1996, *Interpreting Astronomical Spectra* (Chichester: Wiley), 301
- Flower, D. R., Pineau des Forets, G., & Walmsley, C. M. 2007, *A&A*, 474, 923
- Genzel, R., & Downes, D. 1977, *A&AS*, 30, 145
- Gibb, A. G., Thompson, M. A., Wyrowski, F., & Hatchell, J. 2005, *Protostars and Planets V*, 8194
- Herbst, E., & Klemperer, W. 1973, *ApJ*, 185, 505
- Houde, M., Peng, R., Phillips T. G., Bastien, P., & Yoshida, H. 2000, *ApJ*, 537, 245
- Indriolo. N., Geballe, T. R., Oka, T., & McCall, B. J. 2007, *ApJ*, 671, 1736
- Johnston K. J., Heinkel, C., & Wilson, T. L. 1984, *ApJ*, 285, L85

- Kutner, M. L., & Ulich, B. L. 1981, *ApJ*, 250, 341
- Langer, W. D., & Penzias, A. A. 1990, *ApJ*, 357, 477
- Langer, W. D., & Penzias, A. A. 1993, *ApJ*, 408, 539
- Li, H., & Houde, M., 2008, *astro-ph/0801.2757*
- Lintott, C. J., & Rawlings J. M. C. 2006, *A&A*, 448, 425
- Mangum, J. G., Wootten, A., & Mundy, L. G. 1991. *ApJ*, 378, 576
- Mangum J. G., Wooten A., & Mundy L. G. 1992, *ApJ*, 388, 467
- Maret, S., & Bergin, E. A. 2007, *ApJ*, 664, 956
- McCall, B. J., Geballe, T. R., Hinkle, K. H., & Oka, T. 1999, *ApJ*, 522, 338
- Mckee, C. F. 1989, *ApJ*, 345, 782
- Penzias, A. A. 1981, *ApJ*, 249, 518
- Plume, R., Bergin, E. A., Williams, J. P., & Myers, P. C. 1998, in *Chemistry and Physics of Molecules and Grains in Space*, Faraday Discussions, 109, 47
- Polehampton, E. T., Baluteau, J. P., & Swinyard, B. M. 2005, *A&A*, 437, 957
- Richardson, K. J., Sandell, G., Cunningham C. T., Bastien, P., & Davies, S. R. 1994, *A&A*, 286, 555
- Richardson, K. J., White, G. J., & Phillips J. P. 1986, *MNRAS*, 219, 167
- Savage, C., & Ziurys, L. M. 2004, *ApJ*, 616, 966
- Schilke, P., Walmsley, C. M., Millar, T. .J., & Henkel, C. 1991, *A&A*, 247, 487
- Shu, F. H. 1992, *Physics of Astrophysics*, Vol. II (Sausalito: University Science Books), 360
- Solomon, P. M., & Werner, M. W. 1971, *ApJ*, 165, 41
- Stahler, S. W., & Palla, F. 2004, *The Formation of Stars* (Weinheim: Wiley-VCH), 170
- van der Tak, F. F. S., & van Dishoeck, E. F. 2000, *A&A*, 358, L79
- Vastel, C. 2006, URL : <http://www.submm.caltech.edu/~vastel/CASSIS/>
- Watson, W. D. 1974, *ApJ*, 188, 35

Wilson, T. L. & Mauersberger, R. 1990, *A&A*, 239, 305

Woodall, J., Agundez, M., Markwick-Kemper, A. J., & Millar, T. J. 2007, *A&A*, 466, 1197

Woody, D. P., Scott, S. L., Scoville, N. Z., Mundy, L. G., Sargent, A. I., Padin, S., Tinney, C. G., & Wilson, C. D. 1989, *ApJ*, 337, L41

Wootten, A., Snell, R., & Glassgold, A. E. 1979, *ApJ*, 234, 876



Table 1. Data for the observed molecular transitions

Molecular transition	Frequency GHz	$A_{ul}$ $s^{-1}$	$T_{peak}$ K	$V_{peak}$ $km\ s^{-1}$	$\int TdV$ K $km\ s^{-1}$	Velocity range $km\ s^{-1}$	$\tau$
HCNH <sup>+</sup> (3-2)	222.329	$4.61 \times 10^{-6}$	0.062	-3.13	$0.32 \pm 0.02$	(-6.1, 0.3)	0.003
HCNH <sup>+</sup> (4-3)	296.433	$1.13 \times 10^{-5}$	0.064	-3.27	$0.29 \pm 0.02$	(-6.1, -1.3)	0.004
H <sub>3</sub> O <sup>+</sup> (3 <sub>2</sub> -2 <sub>2</sub> )	364.797	$2.79 \times 10^{-4}$	0.16	-3.16	$1.38 \pm 0.08$	(-6.2, 1.2)	0.02
HN <sup>13</sup> C (3-2)	261.263	$6.48 \times 10^{-4}$	0.38	-3.07	$2.99 \pm 0.03$	(-6.7, 1.1)	0.06
HN <sup>13</sup> C (4-3) <sup>a</sup>	348.340	$1.59 \times 10^{-3}$	0.66	-3.81	$6.14 \pm 0.08$	(-10.0, 1.0)	...
H <sup>13</sup> CN (3-2)	259.011	$7.72 \times 10^{-4}$	0.96	-2.84	$8.67 \pm 0.03$	(-9.4, 3.8)	0.09
H <sup>13</sup> CN (4-3)	345.339	$1.9 \times 10^{-3}$	0.39	-2.70	$4.17 \pm 0.02$	(-7.6, 3.5)	0.06
H <sup>13</sup> CO <sup>+</sup> (3-2)	260.255	$1.34 \times 10^{-3}$	1.02	-2.94	$8.37 \pm 0.03$	(-7.4, 2.1)	0.09
H <sup>13</sup> CO <sup>+</sup> (4-3)	346.998	$3.29 \times 10^{-3}$	0.56	-2.70	$4.89 \pm 0.02$	(-7.2, 1.8)	0.07
<sup>13</sup> C <sup>18</sup> O (2-1)	209.419	$5.23 \times 10^{-6}$	0.20	-3.00	$0.91 \pm 0.06$	(-6.1, 0.0)	0.01
<sup>13</sup> C <sup>18</sup> O (3-2)	314.119	$1.89 \times 10^{-6}$	0.22	-3.14	$0.90 \pm 0.03$	(-5.9, -0.9)	0.01
<sup>12</sup> C <sup>18</sup> O (2-1)	219.560	$6.01 \times 10^{-7}$	6.60	-3.14	$41.44 \pm 0.07$	(-7.0, 1.7)	2.19 <sup>c</sup>
<sup>12</sup> C <sup>18</sup> O (3-2) <sup>a</sup>	329.330	$2.17 \times 10^{-6}$	6.06	-3.70	$40.28 \pm 0.12$	(-7.0, 0.6)	...
<sup>13</sup> C <sup>16</sup> O (2-1) <sup>b</sup>	220.398	$6.07 \times 10^{-7}$	...	...	$92.70 \pm 0.14$	(-8.2, 2.8)	...
<sup>13</sup> C <sup>16</sup> O (3-2) <sup>b</sup>	330.587	$2.19 \times 10^{-6}$	...	...	$40.45 \pm 0.32$	(-7.8, 1.9)	...

<sup>a</sup>Not used in the analysis due to shifted  $V_{peak}$ .

<sup>b</sup>Two velocity components, shows strong self-absorption.

<sup>c</sup>optical depth in the center of the line.

Table 2. Rate coefficients<sup>a</sup> of the reactions for H<sub>3</sub><sup>+</sup>, HCNH<sup>+</sup> and HCO<sup>+</sup>

Index <sup>b</sup> (i)	reaction	k <sub>i</sub> (cm <sup>3</sup> s <sup>-1</sup> )
1	H <sub>3</sub> <sup>+</sup> + HCN(HNC) → HCNH <sup>+</sup> + H <sub>2</sub>	8.1 × 10 <sup>-9</sup> (T/300 K) <sup>-0.5</sup>
2	HCO <sup>+</sup> + HCN(HNC) → HCNH <sup>+</sup> + CO	3.1 × 10 <sup>-9</sup> (T/300 K) <sup>-0.5</sup>
3	H <sub>3</sub> O <sup>+</sup> + HCN(HNC) → HCNH <sup>+</sup> + H <sub>2</sub> O	4.0 × 10 <sup>-9</sup> (T/300 K) <sup>-0.5</sup>
4	H <sub>3</sub> <sup>+</sup> + CO → HCO <sup>+</sup> + H <sub>2</sub>	1.7 × 10 <sup>-9</sup>
5 <sup>c</sup>	HCNH <sup>+</sup> + e <sup>-</sup> → (HCN + H) or (HNC + H) or (CN + H + H)	2.8 × 10 <sup>-7</sup> (T/300 K) <sup>-0.65</sup>
6	HCO <sup>+</sup> + e <sup>-</sup> → CO + H	2.4 × 10 <sup>-7</sup> (T/300 K) <sup>-0.69</sup>
10	H <sub>2</sub> <sup>+</sup> + H <sub>2</sub> → H <sub>3</sub> <sup>+</sup> + H	2.1 × 10 <sup>-9</sup>
11 <sup>c</sup>	H <sub>3</sub> <sup>+</sup> + e <sup>-</sup> → (H <sub>2</sub> + H) or (H + H + H)	6.7 × 10 <sup>-8</sup> (T/300 K) <sup>-0.52</sup>

<sup>a</sup>All the rate coefficients are taken from the UMIST database.

<sup>b</sup>The index follows the equation number where the corresponding reaction first appears in the text.

<sup>c</sup>The overall rate coefficient of this reaction is the sum of the rates of all the given branch reactions.

Table 3. Excitation temperatures and column densities

Molecular Species	$T_{ex}$ (K)	$N_{tot}$ ( $\text{cm}^{-2}$ )
HCNH <sup>+</sup>	22	$3.2 \times 10^{13}$
H <sub>3</sub> O <sup>+</sup>	16	$1.3 \times 10^{16}$
HN <sup>13</sup> C	12	$4.4 \times 10^{12}$
H <sup>13</sup> CN	13	$9.8 \times 10^{12}$
H <sup>13</sup> CO <sup>+</sup>	15	$4.8 \times 10^{12}$
<sup>13</sup> C <sup>18</sup> O	20	$9.0 \times 10^{14}$
<sup>12</sup> C <sup>18</sup> O	16	$5.7 \times 10^{16}$
<sup>13</sup> C <sup>16</sup> O	18	$2.9 \times 10^{17}$
<sup>12</sup> C <sup>16</sup> O	...	$1.8 \times 10^{19}$

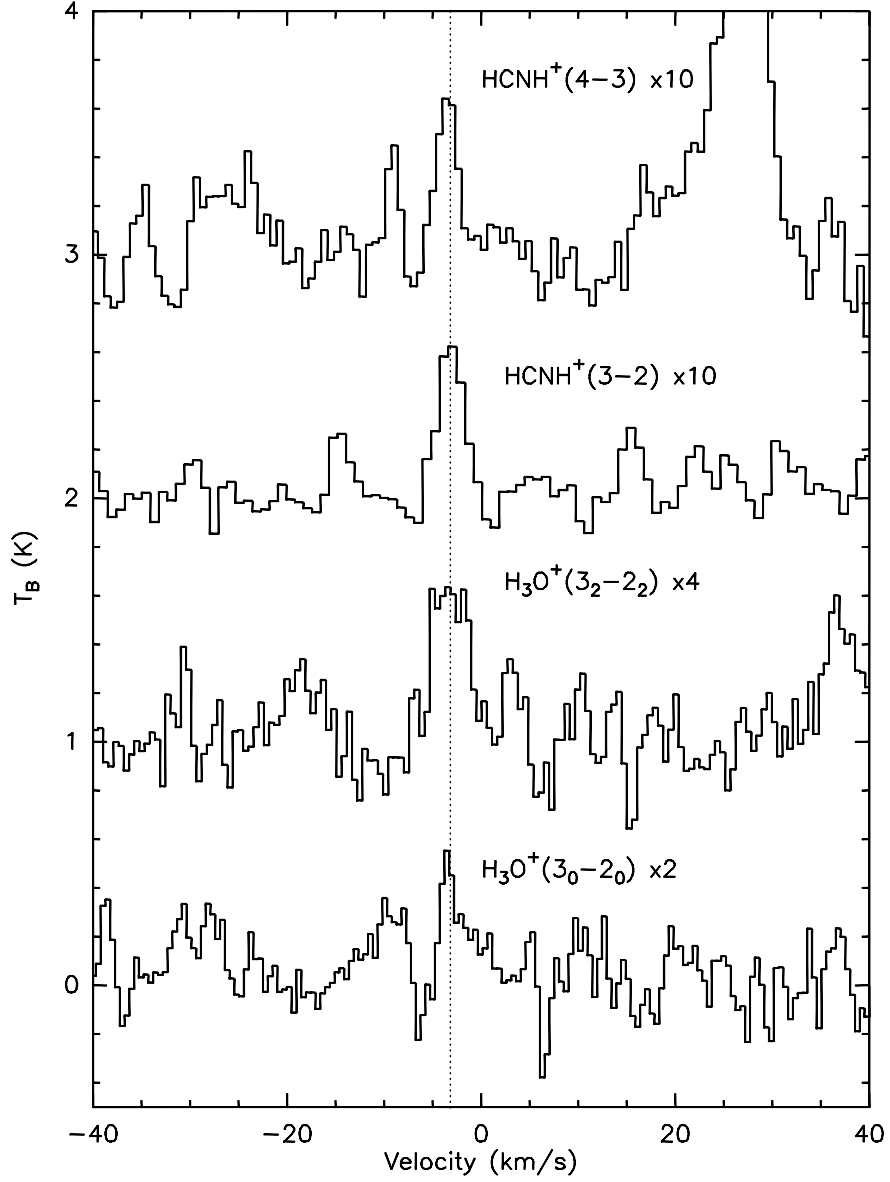


Fig. 1.— The spectra for the  $\text{HCNH}^+$  transitions  $J = 4 \rightarrow 3$  and  $J = 3 \rightarrow 2$ , and para  $\text{H}_3\text{O}^+$  ( $J = 3_2 \rightarrow 2_2$ ) and ortho  $\text{H}_3\text{O}^+$  ( $J = 3_0 \rightarrow 2_0$ ) towards the center position of DR21(OH).

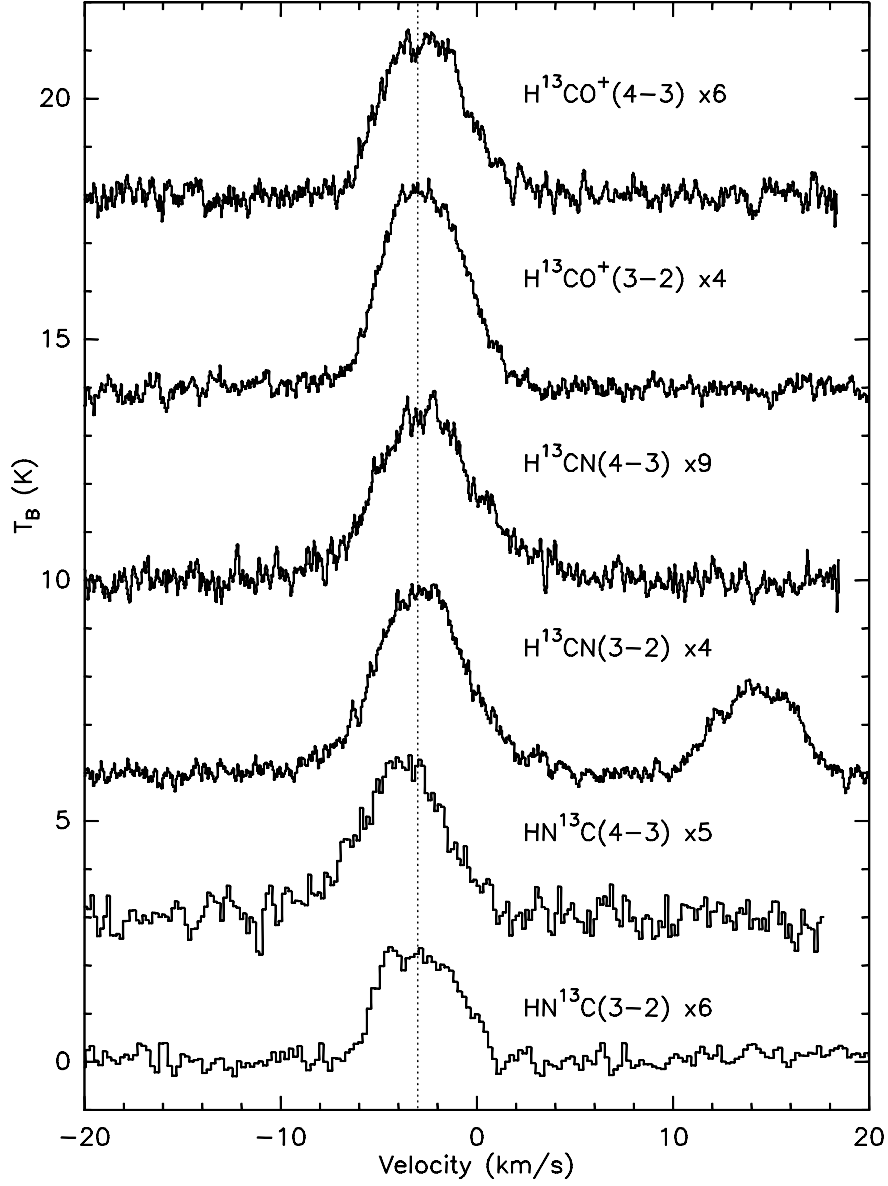


Fig. 2.— The spectra for the  $J = 4 \rightarrow 3$  and  $J = 3 \rightarrow 2$  transitions of  $\text{H}^{13}\text{CN}$ ,  $\text{HN}^{13}\text{C}$ , and  $\text{H}^{13}\text{CO}^+$  towards the center position of DR21(OH).

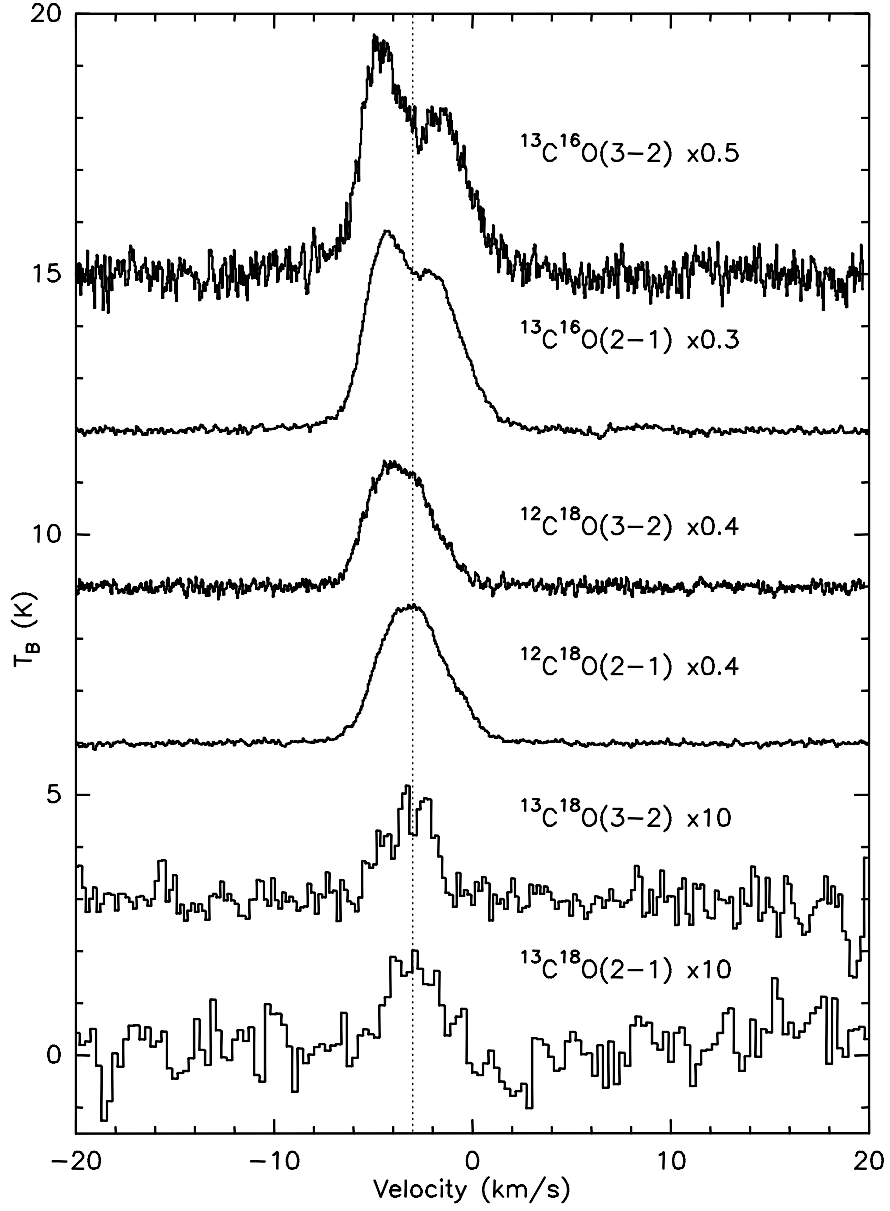


Fig. 3.— The spectra for the  $J = 3 \rightarrow 2$  and  $J = 2 \rightarrow 1$  transitions of  $^{13}\text{C}^{18}\text{O}$ ,  $^{12}\text{C}^{18}\text{O}$ , and  $^{13}\text{C}^{16}\text{O}$  towards the center position of DR21(OH).